Observation of coherence between the photoionization of different inner-shell vacancy states of argon and krypton

J. A. de Gouw,* J. van Eck, A. Q. Wollrabe, J. van der Weg, and H. G. M. Heideman
Debye Institute, Department of Atomic and Interface Physics, Utrecht University, P.O. Box 80.000, 3508 TA Utrecht, The Netherlands
(Received 25 March 1994)

We have observed coherence between the photoionization of the $2s^{-1}(^2S_{1/2})$ and the $2p^{-1}(^2P_{3/2})$ inner-shell vacancy states of argon, and between the $3d^{-1}(^2D_{3/2})$ and the $3d^{-1}(^2D_{5/2})$ inner-shell vacancy states of krypton. The method is based on the occurrence of interferences between photoelectrons and Auger electrons, resulting from the photoionization and subsequent Auger decay of the two states concerned. A parametrization is proposed that describes the observed interference effects reasonably well.

PACS number(s): 32.80.Fb, 32.80.Hd

I. INTRODUCTION

A. Coherence in atomic collisions

An atomic collision process, such as the interaction between an atom and a photon, can usually proceed through many different channels, leading to different final states $|\varphi_n\rangle$. Until a measurement takes place, the final state $|\Phi\rangle$ of the particles after the collision has to be described by a coherent superposition of all the possible final states,

$$|\Phi\rangle = \sum_n t_n |\varphi_n\rangle , \tag{1}$$

in which the summation may also include an integration over continuum states. The expansion coefficients t_n represent the transition amplitudes, which describe the transition to each of the different final states $|\varphi_n\rangle$. In an experiment, one usually selects one of the possible final states $|\varphi_n\rangle$ and measures the cross section for the collision to proceed through that particular channel. The measurement can be interpreted as the projection of the final state $|\Phi\rangle$ upon the final state $|\varphi_n\rangle$, selected by the experimental setup, and the measured cross section is determined by $|t_n|^2$. The transition amplitudes t_n are, in general, complex numbers and by measuring the cross section, no information is obtained on the phase differences, or coherences, between the different amplitudes. A measurement of the coherence between the excitation of two states $|\varphi_n\rangle$ and $|\varphi_m\rangle$ involves an analysis of the interference between the excitation of these states, which is determined by terms of the type $t_n t_m^*$.

Up until now most coherence measurements have been performed on the excitation of degenerate magnetic substates. These measurements are performed using electron-photon or electron-electron coincidence techniques [1]. Coherences between states of different energies are, in general, not easy to observe. For small energy differences they may be observable as quantum beats [2]. For larger energy differences, interferences and hence coherences can only be observed when the different excited states can decay to final states that are indistinguishable. Such a situation occurs, for instance, in the near-threshold electron-impact excitation and subsequent decay of autoionizing states. In this case, the energy distributions of scattered and ejected electrons from different autoionizing states can be made to overlap due to a broadening and an energy shift of these distributions as a result of a postcollision interaction [3–5]. Such an overlap may also be due to a large natural linewidth of two energy distributions as compared with their energy spacing [6,7].

Van den Brink *et al.* [8] have been able to observe coherences between autoionizing states of different energies without employing the natural overlap between such states, or shifting and broadening effects as caused by postcollision interaction. Their method was based on the observation of interferences between scattered and ejected electrons, resulting from the electron-impact excitation and subsequent decay of different autoionizing states, with energy separations of a few eV. A number of experiments have shown striking interference effects in helium [8,9], and in neon and argon [10].

B. Present experiments

In a recent letter [11] we have shown that the method of van den Brink *et al.* can be applied to study the coherences between the photoionization of different inner-shell vacancy states, which can in principle differ in energy by hundreds or even thousands of eV. In the case of

*Present address: Joint Institute for Laboratory Astrophysics, University of Colorado, Boulder, CO 80309-0440.

argon we presented experiments showing the coherence between the photoionization of the $2s^{-1}(^2S_{1/2})$ and the $2p^{-1}(^2P_{3/2})$ states lying as far as 75 eV apart. The purpose of this paper is to describe this experiment in some more detail and furthermore, we will present the results of a new experiment showing the coherence between the $3d^{-1}(^2D_{3/2})$ and the $3d^{-1}(^2D_{5/2})$ states of krypton.

Two different inner-shell photoionized states, $A^+\ n_1\ell_1^{-1}$ and $A^+\ n_2\ell_2^{-1}$ plus the corresponding photoelectrons, can decay to the same final state by tuning the photon energy $h\nu$ such that in the following two processes:

$$h\nu + A \longrightarrow \begin{cases} A^+\ n_1\ell_1^{-1} + e_{\rm ph}^{(1)} \longrightarrow A^{2+} + e_A^{(1)} + e_{\rm ph}^{(1)} \\ A^+\ n_2\ell_2^{-1} + e_{\rm ph}^{(2)} \longrightarrow A^{2+} + e_A^{(2)} + e_{\rm ph}^{(2)}, \end{cases} \tag{2}$$

the energy of the photoelectron $e_{\rm ph}^{(1)}$ becomes equal to the energy of the Auger electron $e_A^{(2)}$, and, consequently (if the doubly ionized A^{2+} state is the same for both channels), the energy of the photoelectron $e_{\rm ph}^{(2)}$ becomes equal to the energy of the Auger electron $e_A^{(1)}$. In that case it is not possible to decide from the detection of an electron whether it was an Auger electron from one channel or a photoelectron from the other, and, therefore, interference between these two possibilities is expected to occur. This interference not only depends on the coherence between the two transition amplitudes describing the photoionization process to the $A^+\ n_1\ell_1^{-1}$ and the $A^+\ n_2\ell_2^{-1}$ states, but also on the transition amplitudes describing the Auger decay of the $A^+\ n_1\ell_1^{-1}$ and the $A^+\ n_2\ell_2^{-1}$ states to the A^{2+} state plus an Auger electron.

As mentioned before, in our system of photoionization and subsequent Auger decay it is possible to study coherences between the transition to states that are widely separated in energy. Apart from that, our system has several advantages, but also some disadvantages, as compared with the system of electron-impact excitation of an autoionizing state in the work of van den Brink *et al.*

The first advantage is the fact that photoionization and, to a lesser extent, Auger decay, are phenomena that are much simpler from a theoretical point of view than electron-impact excitation of an autoionizing state. Photoionization can be described in the dipole approximation and this restricts the number of orbital angular momenta of the photoelectrons to one in case of s vacancies and to two for vacancies with a higher orbital angular momentum. The second advantage is the fact that in the case of photoionization the contribution of the direct double-ionization channel is negligible, whereas in the experiment of van den Brink *et al.* the contribution of the direct single-ionization channel is quite large. Such a direct channel, leading to the same final state, interferes with the two indirect channels, and hence makes the system more complicated. These two advantages allow an important simplification of the qualitative theory as given by van den Brink *et al.* [9] to describe the observed interference phenomena. Moreover, these advantages promise the possibility to do *ab initio* calculations that can be quantitatively compared with our experiment, whereas it will be very hard to do a calculation that can quantitatively explain the interference phenomena seen in the experiment of van den Brink *et al.* These advantages as compared with the earlier experiments are the main motivations for the work presented in this paper. The third advantage is the polarization of the synchrotron radiation, which gives an extra experimental possibility, whereas the experiments of van den Brink *et al.* were done with a nonpolarized electron beam.

The main disadvantage of the system of photoionization and subsequent Auger decay is the fact that an inner-shell vacancy state can, in general, decay to many different doubly ionized states. To elucidate this we refer to the processes as given in (2). Suppose the electron spectrometer is tuned to transmit electrons with energies equal to the energy of the Auger electron $e_A^{(1)}$. If then in the coherence experiment an electron is detected, it may have been the Auger electron $e_A^{(1)}$ or the photoelectron $e_{\rm ph}^{(2)}$. Of course, these two possibilities cannot be distinguished, which accounts for the interference between the two electrons. If the detected electron was the Auger electron $e_A^{(1)}$, the whole process of ionization to the $A^+\ n_1\ell_1^{-1}$ state and decay to the A^{2+} state is fully determined. However, if the detected electron was the photoelectron $e_{\rm ph}^{(2)}$, only the ionization process to the $A^+\ n_2\ell_2^{-1}$ state is determined, but this state need not necessarily decay to the particular final state that leads to interference. Therefore, there is an important contribution of noncoherent processes, which can be overcome in a coincidence experiment, in which both electrons are detected, or by looking for a suitable combination of states in which the inner-shell vacancy has a nearly 100% probability to decay to a certain final state, like in the experiments of van den Brink *et al.* In their system of excitation and subsequent decay of, for instance, helium, the probability for a doubly excited, autoionizing state to decay to the ground state of He^+ is nearly 100%.

In this paper, first the qualitative theoretical description as given by van den Brink *et al.* [9] to describe the interference phenomena will be summarized and adapted to our system of photoionization and subsequent Auger decay. Next, we will present the results of the experiments, in which the coherences between the photoionization of two different inner-shell vacancy states are studied in the cases of argon and krypton.

II. THEORETICAL DESCRIPTION

Van den Brink *et al.* [9] have been able to give a qualitative description of the interference effects between scattered and ejected electrons resulting from the electron-impact excitation and subsequent decay of different autoionizing states. The advantages of working with inner-shell photoionization and Auger decay, as discussed in the introduction, lead to a number of simplifications in this theory. In this section, we will discuss these simplifications and their implications on the parametrization

of the structures resulting from the interference between photoelectrons and Auger electrons. Recently, the theory of such interference effects has also been discussed by Végh and Macek [12] for the case of interferences between photoelectrons and Auger electrons resulting from the photoionization of the same inner-shell vacancy state, and by Végh [13] for the case of interferences between photoelectrons and Auger electrons resulting from different inner-shell vacancy states. Only in the latter case the coherences between the photoionization of different inner-shell vacancy states are of importance in the theory.

A. The Auger effect in the context of resonance scattering

The theory of van den Brink *et al.* [9] is an extension of the well-known work of Fano [14], and Fano and Cooper [15], who described the excitation and subsequent decay of an autoionizing state in the broader context of resonance scattering. Such theories account for the fact that the final state after electron-impact excitation and subsequent decay of an autoionizing state can, in general, also be reached through an alternative channel, which consists of the direct ionization process. The interference between both channels leads to a typical resonance structure, the so-called Fano profile, in the cross section for electron-impact ionization at the scattered and ejected electron energies.

Van den Brink *et al.* [9] arrive at an alternative parametrization to describe the cross section in a resonance. The doubly differential cross section for the emission of an electron with energy E from an autoionizing state $|a\rangle$ reads in their case

$$\frac{d^2\sigma}{dEd\Omega} = Q^2\left\{1 + P_a e^{-i\phi_a}\sin\delta_a e^{-i\delta_a} + \text{c.c.}\right\}, \tag{3}$$

in which c.c. means the complex conjugate of the preceding term, and Q^2 is the direct-ionization cross section far from resonance. The parameters P_a and ϕ_a represent the amplitude and the phase of the resonance contribution, and are, just as Q^2, assumed to vary negligibly within the energy width of the resonance. The phase shift δ_a is defined by

$$\cot\delta_a \equiv \frac{E_r^a - E}{\Gamma_a/2}, \tag{4}$$

in which E_r^a is the energy position and Γ_a the width of the resonance. It can be seen that δ_a varies rapidly through π when E traverses the resonance energy. From Eq. (4) it follows that

$$-\sin\delta_a e^{-i\delta_a} = \frac{\Gamma_a/2}{E - E_r^a - i\Gamma_a/2}. \tag{5}$$

If we substitute this equation in (3) we arrive at

$$\frac{d^2\sigma}{dEd\Omega} = Q^2\left(1 - \frac{2P_a\bar{\epsilon}\cos\phi_a + 2P_a\sin\phi_a}{\bar{\epsilon}^2+1}\right), \tag{6}$$

in which we have introduced the reduced energy $\bar{\epsilon}$, defined as

$$\bar{\epsilon} = \frac{E - E_r^a}{\Gamma_a/2}. \tag{7}$$

From Eq. (6) it can be seen that the cross section consists of a (nearly) constant background Q^2, a symmetric and an antisymmetric resonance part, the relative contributions of which are determined by the phase ϕ_a.

Earlier, photoionization and subsequent Auger decay have also been described in the context of resonance scattering [16], which justifies the application of the description of van den Brink *et al.* to the present system. In our system the indirect channel consists of inner-shell photoionization and subsequent Auger decay, whereas the direct channel consists of the double-photoionization process. Indeed, if the direct and indirect channel are of a comparable strength, an asymmetric resonance profile as given by (3) and (6) may be observed in the double-photoionization cross section at energies pertaining to the photoelectrons and Auger electrons, but, up until now, this has only been observed in a few cases [17,18]. Usually, the cross section for direct double photoionization is negligibly small and, therefore, the energy distribution of the Auger electrons has a Lorentzian line shape on a negligible background. In that case, the resonance line shape as given by Eq. (6) can be simplified to a Lorentzian by substituting $P_a \gg 1$ and $\phi_a = -\pi/2$ resulting in

$$\frac{d^2\sigma}{dEd\Omega} = \frac{2Q^2P_a}{\bar{\epsilon}^2+1}. \tag{8}$$

In deriving this equation we have neglected the influence of post-collision interaction (PCI). In the present experiments the excess energy of the photon is, in general, of the same magnitude as the Auger-electron energy and, therefore, the influence of PCI can indeed be neglected, as has been shown by Borst and Schmidt [19].

B. Interference between photoelectrons and Auger electrons

We now proceed to extend the theory of van den Brink *et al.* [9] to describe the interference between photoelectrons and Auger electrons, resulting from the photoionization and subsequent Auger decay of two different inner-shell vacancy states. As seen above, in the two following processes:

$$h\nu + A \longrightarrow \begin{cases} A^+\ n_1\ell_1^{-1} + e_{\text{ph}}^{(1)} & \longrightarrow A^{2+} + e_A^{(1)} + e_{\text{ph}}^{(1)} \\ A^+\ n_2\ell_2^{-1} + e_{\text{ph}}^{(2)} & \longrightarrow A^{2+} + e_A^{(2)} + e_{\text{ph}}^{(2)}, \end{cases}$$

the photon energy $h\nu$ can be chosen such that the energy of the photoelectron $e_{\text{ph}}^{(1)}$ becomes equal to the energy of the Auger electron $e_A^{(2)}$, and consequently the energy of the photoelectron $e_{\text{ph}}^{(2)}$ becomes equal to the energy of the Auger electron $e_A^{(1)}$. In that case, the final state of the two processes cannot be distinguished and interferences between the two possibilities are expected to occur. To

describe these interferences we need an expression for the amplitude describing the transition from the ground state of the atom plus the photon with energy $h\nu$, to a final state with two free electrons with energies E and E' and directions Ω and Ω', respectively, which accounts properly for the two different channels that lead to this final state. Following van den Brink *et al.* we introduce two matrix elements of a suitable transition operator T,

$$T_1 \equiv \langle E\Omega; E'\Omega' \mid T \mid h\nu \rangle , \tag{9}$$

$$T_2 \equiv \langle E'\Omega'; E\Omega \mid T \mid h\nu \rangle . \tag{10}$$

T_1 is the matrix element describing the transition to a final state with a photoelectron (E, Ω) and an Auger electron (E', Ω'), whereas T_2 describes the complementary process resulting in a final state with a photoelectron (E', Ω') and an Auger electron (E, Ω). It should be noted that the energies E and E' of the two electrons are related due to energy conservation,

$$E + E' = h\nu - E_i, \tag{11}$$

in which E_i is the energy of the final doubly ionized state.

In the theory of van den Brink *et al.* the exact formulation of the operator T remains unspecified, but in our system of photoionization and subsequent Auger decay, the matrix elements T_1 and T_2 can simply be given as [12,13,16]

$$T_1 = \frac{\langle E'\Omega' \mid V_{\rm el} \mid a \rangle \langle a; E\Omega \mid H_{\rm int} \mid h\nu \rangle}{E' - E'^{a}_{r} + i\Gamma_a/2}, \tag{12}$$

$$T_2 = \frac{\langle E\Omega \mid V_{\rm el} \mid a' \rangle \langle a'; E'\Omega' \mid H_{\rm int} \mid h\nu \rangle}{E - E^{a'}_{r} + i\Gamma_{a'}/2}, \tag{13}$$

in which $|a\rangle$ and $|a'\rangle$ denote the two inner-shell vacancy states, with energy widths Γ_a and $\Gamma_{a'}$ and resulting Auger energies E^a_r and $E^{a'}_r$, respectively. The right-hand parts of the two matrix elements represent the inner-shell photoionization process, in which the Hamiltonian $H_{\rm int}$ for the interaction between the photon and the atom can be approximated by the dipole operator. The left-hand parts represent the Auger decay, in which the operator $V_{\rm el}$ can be taken as the Coulomb repulsion between all interacting electron pairs. In the derivation of Eqs. (12) and (13) the direct double-photoionization process has been neglected and also the postcollision interaction between the photoelectron and Auger electron is not taken into account [12,13,16].

Returning to the derivation of van den Brink *et al.* we can now write for the relevant state $|\Psi_a\rangle$ of the two final electrons (labeled 1 and 2)

$$|\Psi_a\rangle \sim (T_1 - T_2) \times \frac{|E\Omega(1)\rangle\,|E'\Omega'(2)\rangle - |E'\Omega'(1)\rangle\,|E\Omega(2)\rangle}{\sqrt{2}}. \tag{14}$$

To account for interference, this expression is properly antisymmetrized with respect to $1 \leftrightarrow 2$ permutation. The triply differential cross section for the transition to a final state with two electrons (E, Ω) and (E', Ω') can now be given as

$$\frac{d^3\sigma}{d\Omega d\Omega' dE} = \langle \Psi_a \mid \Psi_a \rangle \sim |T_1 - T_2|^2 . \tag{15}$$

Until this point, the spin states of the two outgoing electrons have not been considered in the theory. However, the spin is important, since the total final state, including the spin state, has to be antisymmetric for $1 \leftrightarrow 2$ permutations. In the experiment we do not observe the spin states of the electrons and, therefore, the observed interference term will be smaller than expressed in (15). Following van den Brink *et al.* we find for the case in which the two electrons are, for instance, coupled to a singlet state

$$\frac{d^3\sigma}{d\Omega d\Omega' dE} \sim \left[\tfrac{1}{2}\,|T_1 - T_2|^2 + \tfrac{1}{2}\,|T_1|^2 + \tfrac{1}{2}\,|T_2|^2\right]. \tag{16}$$

The dependence of the cross section on the photon and electron energy is fully specified by the equations above. In order to describe the angle dependence of the cross section, the angular part of the wave functions for the two outgoing electrons can be expanded in spherical harmonics. An important simplification arises in this expansion, since for the photoelectron wave functions only a limited number of partial waves has to be considered. Due to the applicability of the dipole approximation and due to the conservation of parity, a photoelectron ejected from an inner shell with orbital angular-momentum quantum number ℓ can only have an angular momentum specified by $\ell - 1$ or $\ell + 1$ in the continuum state. More details on this expansion of the angular part of the wave functions in spherical harmonics are given by van den Brink *et al.* [9], by Végh and Macek [12] and by Végh [13].

In our (noncoincidence) experiment only one electron is detected, which is either the Auger or the photoelectron. This implies that the detection of photoelectrons (Auger electrons) is integrated over all directions of the corresponding Auger electrons (photoelectrons). The theoretical cross section (16) must, therefore, also be integrated over all directions of the unobserved electron before it can be compared to the experiment. This integration yields zero interference terms for spherical harmonics with different ℓ values. Consequently, interferences between Auger and photoelectrons can only be observed if, in addition to their energies, also their orbital angular momenta are the same.

The theory of van den Brink *et al.* [9] finally arrives at a parametrization for the cross section that accounts for the interference between scattered and ejected electrons resulting from the electron-impact excitation and subsequent decay of two different autoionizing states

$$\begin{aligned}\frac{d^2\sigma}{dEd\Omega} = Q^2(1 &+ P_a e^{-i\phi_a} \sin\delta_a e^{-i\delta_a} + \text{c.c.} \\ &+ P_{a'} e^{-i\phi_{a'}} \sin\delta_{a'} e^{-i\delta_{a'}} + \text{c.c.} \\ &+ P_{a,a'} e^{-i\phi_{a,a'}} \sin\delta_a e^{-i\delta_a} \sin\delta_{a'} e^{+i\delta_{a'}} + \text{c.c.}),\end{aligned} \tag{17}$$

in which the phase shifts δ_a and $\delta_{a'}$ are defined in a similar way as in Eq. (4). The equation contains the following four terms:

(1) A background due to the direct ionization process.

(2) A resonance profile with amplitude P_a and phase ϕ_a pertaining to the scattered electrons from state $|a\rangle$.

(3) A resonance profile with amplitude $P_{a'}$ and phase $\phi_{a'}$ pertaining to the ejected electrons from state $|a'\rangle$.

(4) An interference term, with amplitude $P_{a,a'}$ and phase $\phi_{a,a'}$. This phase is the relative phase between the ejected- and scattered-electron amplitudes. It contains the coherence between $|a\rangle$ and $|a'\rangle$ plus an additional phase, which depends on the autoionizing decay.

When applied to our system of photoionization and Auger decay, we can again modify this parametrization in two ways. First, the direct channel consists in our case of the direct double-photoionization process, which is negligibly small. This means that the parameters P_a, $P_{a'}$, and $P_{a,a'}$ are all much larger than one. Second, the line shapes pertaining to the photoelectrons and Auger electrons are Lorentzians, which means that we again may put $\phi_a = \phi_{a'} = -\pi/2$. Using these modifications plus our Eqs. (5) and (6) we can simplify the parametrization (17). We now have for the cross section for the emission of an electron, either the photoelectron or the Auger electron, at an energy E and a direction Ω

$$\frac{d^2\sigma}{dEd\Omega} = Q^2\left(\frac{2P_a}{\bar{\epsilon}_a^2+1} + \frac{2P_{a'}}{\bar{\epsilon}_{a'}^2+1} + \frac{2P_{a,a'}(\bar{\epsilon}_a\bar{\epsilon}_{a'}+1)\cos\phi_{a,a'} + 2P_{a,a'}(\bar{\epsilon}_{a'}-\bar{\epsilon}_a)\sin\phi_{a,a'}}{(\bar{\epsilon}_a^2+1)(\bar{\epsilon}_{a'}^2+1)}\right) \tag{18}$$

in which P_a and $P_{a'}$ are now the amplitudes for the photoelectrons and Auger electrons, respectively, and in which Q^2 is now the cross section for the direct double-photoionization process far from resonance. Although it is assumed that Q^2 is very small, this does not mean that also the amplitudes P_a, $P_{a'}$, and $P_{a,a'}$ times Q^2 can be neglected. The reduced energies $\bar{\epsilon}_a$ and $\bar{\epsilon}_{a'}$ are defined, similarly as before, by

$$\bar{\epsilon}_a = \frac{E - E_r^a}{\Gamma_a/2},$$

$$\bar{\epsilon}_{a'} = \frac{E - E_r^{a'}}{\Gamma_{a'}/2}.$$

Far from resonance both $\bar{\epsilon}_a$ and $\bar{\epsilon}_{a'}$ are very large and the expression (18) yields a zero cross section. When one of the reduced energies is near zero, that is, if either Auger or photoelectrons are detected, the expression (18) is equivalent to a single Lorentzian line shape. Only when both $\bar{\epsilon}_a$ and $\bar{\epsilon}_{a'}$ are near zero, the interference term arises, which is the case when both Auger and photoelectrons are detected.

To give some insight in the possible interference patterns that are predicted by the theory, we have plotted the cross section according to the parametrization (18) as a function of both the photon and the electron detection energy, in the region where the photoelectron and Auger-electron energies are about equal. The detection energy is varied through the position of the Auger line, whereas the photon energy is varied through the region where the photoelectrons from $|a\rangle$ have about the same energies as the Auger electrons from $|a'\rangle$. The results are shown in Fig. 1. The height of the surfaces in this figure gives the cross section for the detection of an electron, either the photoelectron or the Auger electron. If there is no interference between photoelectrons and Auger elec-

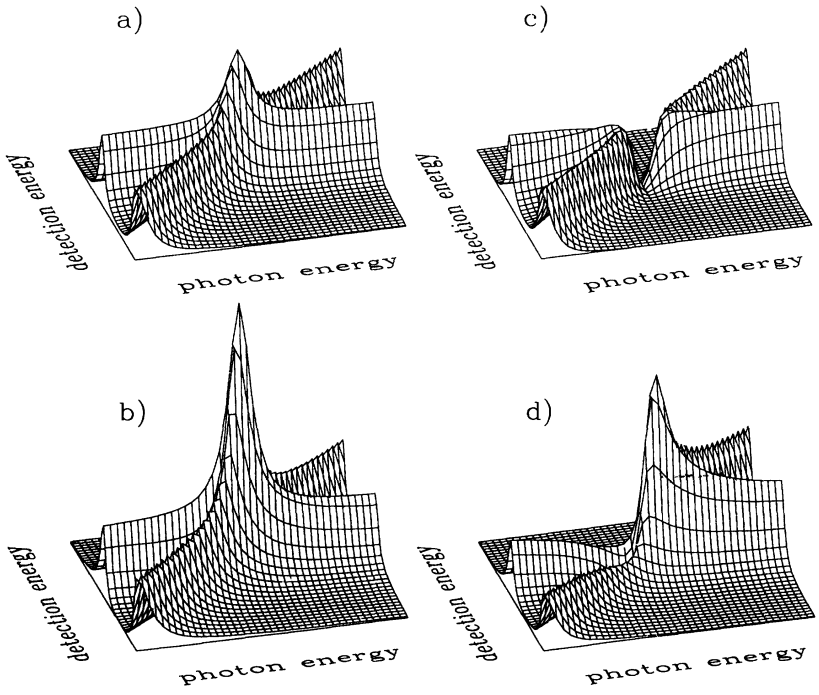

FIG. 1. The cross section for the detection of an electron according to the proposed parametrization (18) in the region where the photoelectrons and Auger electrons have about the same energies: (a) $P_a = P_{a'} = 2$, $P_{a,a'} = 0$; (b) $P_a = P_{a'} = 2$, $P_{a,a'} = 0.25$, $\phi_{a,a'} = 0$; (c) $P_a = P_{a'} = 2$, $P_{a,a'} = 0.25$, $\phi_{a,a'} = \pi$; (d) $P_a = P_{a'} = 2$, $P_{a,a'} = 0.25$, $\phi_{a,a'} = -\pi/2$.

trons we put $P_{a,a'}$ equal to zero, which results in the cross section according to Fig. 1(a). The energy of the Auger electrons does not depend on the photon energy, which is represented by the Lorentzian-shaped ridge parallel to the photon-energy axis. The energy of the photoelectrons depends linearly on the photon energy, which is represented by the Lorentzian-shaped ridge at an angle of 45° to the photon-energy axis in Fig. 1(a). In the region where both ridges cross, the photoelectrons and Auger electrons cannot be distinguished, but in this case there is no interference and, therefore, the two ridges just add up incoherently, resulting in a peak with twice the height of the ridges pertaining to the photoelectrons and Auger electrons.

In Fig. 1(b) we have plotted the cross section with an interference term. The phase $\phi_{a,a'}$ of the interference has been taken equal to zero in this case. It can be seen that in the region where the ridges pertaining to the photoelectrons and Auger electrons cross, they add up to more than twice (four times) the original heights. This corresponds to maximum constructive interference.

In Fig. 1(c) we have plotted the cross section with an interference term, but now the phase $\phi_{a,a'}$ has been taken equal to π. In the region where photoelectrons and Auger electrons are indistinguishable, the cross section has a minimum equal to zero, which corresponds to completely destructive interference.

Figure 1(d) shows the cross section with an interference term for $\phi_{a,a'} = -\pi/2$, which results in a more complex asymmetric pattern. It can be seen that a one-dimensional cut through this surface parallel to the photon-energy axis resembles a typical asymmetric resonance profile with a peak and a dip. In the measurement of a spectrum the electron yield is usually measured at a constant detection energy, at a constant photon energy or at a constant energy loss, defined as the photon energy minus the detection energy, which corresponds to taking one-dimensional cuts through the surfaces in Fig. 1, in directions parallel to the detection-energy axis, the photon-energy axis or the diagonal, respectively.

III. THE EXPERIMENTAL SETUP

The measurements were performed with a setup combining synchrotron radiation as a photon source and an extended cylindrical mirror analyzer (CMA) as an electron spectrometer. This setup has been described elsewhere in detail [20], but a brief outline will be given below.

The photon source consists of the undulator beam line at the Synchrotron Radiation Source of the Daresbury Laboratory. This beam line combines a reasonable photon flux (10^{11} photons/s) with a high energy resolution (0.05% of the photon energy). The photon beam is refocused by a combination of a spherical and an ellipsoidal mirror, resulting in a focus point of 0.5×1.0 mm^2.

Our CMA has two extensions as compared with a conventional CMA. First, to improve the energy resolution at high electron energies, the electrons can be retarded before they enter the CMA, which is done by applying a retarding potential over two half spheres. The energy resolution is about 0.7% of the electron energy that is transmitted by the CMA. Therefore, by retarding electrons of 40 eV (in the experiments on krypton) to 10 eV, an energy resolution of about 0.07 eV is achieved. Second, we can also obtain information on the angular distribution of the electrons, which is achieved by detecting electrons emitted in different directions on different sectors of a channel plate. In the present experiments we have not used this possibility, but, instead, just added up the signals of the different sectors of the channel plate. More details on our detection system can be found elsewhere [20].

IV. EXPERIMENTS ON ARGON

Argon is the smallest noble-gas atom with more than one inner shell and provides, therefore, the simplest system for the study of coherences between the photoionization of different inner-shell vacancy states.

In the experiment presented in this section we have concentrated on the study of the coherences between the $2s^{-1}(^2S_{1/2})$ state (binding energy E_B=326.5 eV [21]) and the $2p^{-1}(^2P_{3/2})$ (E_B=248.63 eV [22]) inner-shell vacancy states of argon. These two states (plus the corresponding photoelectrons) can decay to the same final state in the following way:

$$h\nu + \mathrm{Ar} \rightarrow \mathrm{Ar}^+\, 2s^{-1}(^2S_{1/2}) + \underset{\ell=1}{e_{\mathrm{ph}}^{(1)}} \rightarrow \mathrm{Ar}^{2+}\, 3p^{-2}(^1D_2) + \underset{\ell=2}{e_A^{(1)}} + \underset{\ell=1}{e_{\mathrm{ph}}^{(1)}}$$

$$h\nu + \mathrm{Ar} \rightarrow \mathrm{Ar}^+\, 2p^{-1}(^2P_{3/2}) + \underset{\ell=0,2}{e_{\mathrm{ph}}^{(2)}} \rightarrow \mathrm{Ar}^{2+}\, 3p^{-2}(^1D_2) + \underset{\ell=1,3}{e_A^{(2)}} + \underset{\ell=0,2}{e_{\mathrm{ph}}^{(2)}}.$$

By adjusting the photon energy such that the energy of the photoelectron $e_{\mathrm{ph}}^{(1)}$ becomes equal to the energy of the Auger electron $e_A^{(2)}$ and vice versa, the final states of the two processes become indistinguishable and interferences are expected to occur. In the previous section it was seen that, in order to possibly observe interference, not only the energies of the photoelectrons and Auger electrons should be the same, but also their orbital angular momenta. From the quantum numbers for the orbital angular momentum, indicated below the two processes, it is clear that this condition can be met for the two channels that we have chosen.

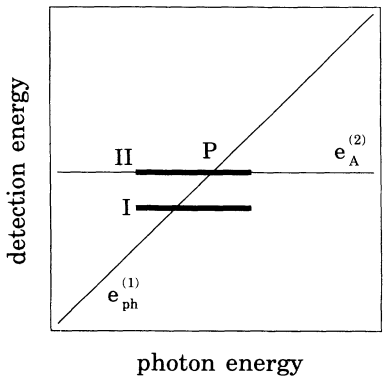

FIG. 2. The energies of photoelectrons ($e_{ph}^{(1)}$) and Auger electrons ($e_A^{(2)}$) as a function of the photon energy. At the intersection P the proposed interference should be observable. The bold lines I and II indicate the way in which we have performed two photon-energy scans which are referred to as measurement I and II (see text).

A. Experiment

The expected interference should be visible in the detection of the indistinguishable electrons $e_{ph}^{(1)}$ and $e_A^{(2)}$ on the one hand, and in the detection of electrons $e_{ph}^{(2)}$ and $e_A^{(1)}$ on the other hand. We have chosen to study the interference between $e_{ph}^{(1)}$ ($2s^{-1}$ photoelectrons) and $e_A^{(2)}$ [$L_3 - M_{23}M_{23}$ ($^1D_2$) Auger electrons], rather than between $e_{ph}^{(2)}$ and $e_A^{(1)}$, since the Auger-electron signal from the Ar^+ $2s^{-1}$ state ($e_A^{(1)}$) is rather small.

Figure 2 illustrates the way in which we have performed the measurements. The energies of the Auger and the photoelectrons are shown as a function of the photon energy. The Auger electrons have an energy of 203.49 eV [23] which is independent of the photon energy and are, therefore, represented by the horizontal line. The photoelectrons have an energy equal to the photon energy minus the binding energy (326.5 eV) of the $2s$ inner-shell electron and are, therefore, represented by the diagonal line. At point P the two lines intersect and the Auger and photoelectrons become indistinguishable. The bold lines I and II indicate the way in which we have performed two photon-energy scans, which we will call measurement I and II. In both measurements the detection energy (E_d) of the electron analyzer is kept constant and the electron yield is measured as a function of the photon energy. Measurement I will show a peak consisting of photoelectrons only, whereas measurement II will show a photoelectron peak on a "background" of Auger electrons. Hence, interference effects should be visible in measurement II.

The electron energy in the present experiment is typically 200 eV. By retarding the electrons to 50 eV a resolution of about 0.4 eV is achieved. The photon energy is typically 530 eV, with a bandwidth of about 0.27 eV.

B. Results and discussion

Figure 3 shows the results of the measurements. Measurement I, according to scan I in Fig. 2, is shown in

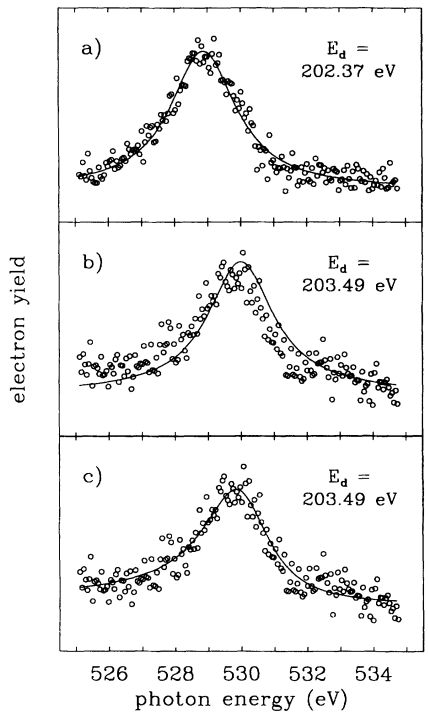

FIG. 3. (a) Ar^+ $2s^{-1}$ photoelectrons ($e_{ph}^{(1)}$) as a function of the photon energy at a detection energy of 202.37 eV, (b) Ar^+ $2s^{-1}$ photoelectrons at a detection energy of 203.49 eV. In this case the background contains Ar $L_3 - M_{23}M_{23}$ ($^1D_2$) Auger electrons. The solid line indicates a fit without interference. (c) Same measurement as in (b) but the solid line represents a fit using a parametrization containing state-state interference.

Fig. 3(a). The detection energy is set to 202.37 eV. This energy does not correspond to any Auger energy. The measurement is the sum of two separate measurements, each of which took about two hours. The solid line indicates a least-squares fit ($\chi^2 = 1.22$) of a Lorentzian line shape to the data. It is seen that the line agrees well with the data. The peak position of the line was found to be 528.87±0.02 eV and the peak width 2.44±0.09 eV. To determine the width of the Ar^+ $2s^{-1}(^2S_{1/2})$ state we have to consider both the transmission profile of the electron analyzer and the energy profile of the photon beam. In our previous letter [11] we reported a resulting value of 1.9±0.2 eV for the linewidth, but by that time we had only limited knowledge of the transmission profiles. In the meantime we have measured both the transmission profile of the electron analyzer and the energy profile of the photon beam and by deconvoluting the measured Ar^+ $2s^{-1}(^2S_{1/2})$ line shape with these profiles, we found a linewidth of 2.27±0.08 eV, the small error being due to the improved statistics in these measurements. It can be seen that our former estimate of the linewidth was too small, but the present value is in perfect agreement with both the most recent experimental value of 2.25 eV [24] and the most recent theoretical value of 2.3 eV [25].

Measurement II, according to scan II in Fig. 2, is shown in Fig. 3(b). The detection energy is now 203.49 eV, which corresponds to the energy of the L_3 −

$M_{23}M_{23}$ ($^1D_2$) Auger electrons. Again this is the sum of two separate measurements, each of which took three hours. It is important to point out that only the detection energy is different from that in measurement I. This is achieved by changing the potential on the retarding spheres, which can be done very accurately by a computer-controlled digital-to-analog converter. The other potentials as well as the photon-energy interval are left unchanged. If we assume that interference between Auger and photoelectrons does not occur, measurement II [Fig. 3(b)] should exhibit the following two features:

(1) The position of the photoelectron peak should change relative to its position in measurement I by the same amount as the change in detection energy. The detection energy is changed by 1.12 eV. The peak position should, therefore, be at 529.99 eV.

(2) The ratio between the photoelectron peak and the "background" is known beforehand and should be 6.79. The background in measurement II consists of Auger electrons and experimental noise. The ratio of the noise to the photoelectron peak can be found from measurement I, and was found to be 1.86. Moreover, this ratio appeared to be independent of the photon flux, which decreases gradually during a measurement. The Auger to photoelectron peak ratio was determined by taking a spectrum in which both Auger and photoelectrons can be seen. This measurement, which is not shown here, gave an Auger to photoelectron ratio of 4.93. In measurement II the background to peak ratio should, therefore, be 1.86+4.93=6.79.

In Fig. 3(b) the solid line indicates a least-squares fit ($\chi^2 = 2.44$) to the data of a Lorentzian line shape, which satisfies both conditions mentioned above: the peak position is held fixed at 529.99 eV and the background to peak ratio is taken to be 6.79. The width of the line is again taken to be 2.44 eV. Only the multiplication factor of the whole curve is a variable parameter. It is clear that the line does not agree very well with the data. The experimentally found peak position is shifted relative to the position where it should be. Also, the symmetrical line shape of the fit is not in agreement with the asymmetrical shape of the experimental data. We attribute the differences between the measurement and the Lorentzian fit to the interference between the Auger and the photoelectrons. In the following we will show that measurement II can be described much better by including interference.

In measurement II the electron yield is measured as a function of the photon energy, but the detection energy is held constant and is equal to the energy of the Auger electrons. In the parametrized line shape as given by our Eq. (18) we may, therefore, substitute $E = E_r^{a'}$ (or $\bar{\epsilon}_{a'} = 0$), which results in

$$\frac{d^2\sigma}{dEd\Omega} = Q^2\left(\frac{2P_a}{\bar{\epsilon}_a^2+1} + 2P_{a'} + \frac{2P_{a,a'}\cos\phi_{a,a'} - 2P_{a,a'}\bar{\epsilon}_a\sin\phi_{a,a'}}{\bar{\epsilon}_a^2+1}\right). \quad (19)$$

This expression contains three terms, the first representing the Lorentzian profile pertaining to the photoelectrons, the second the constant background pertaining to the Auger electrons and the third representing the interference term.

The ratio between $P_{a'}$ and P_a is known and equal to 4.93, as has been argued above. Figure 3(c) shows again measurement II, but now with the solid line representing a least-squares fit ($\chi^2 = 1.09$) to the data of the parametrized line shape containing interference according to Eq. (19). The only free parameters are $P_{a,a'}/P_a$ and $\phi_{a,a'}$. The known resonance position E_r^a is held fixed at 529.99 eV and the width Γ_a is taken equal to 2.44 eV, as found from measurement I. It is clear that the measurement is much better described by the parametrization, which includes interference between Auger and photoelectrons. For the relevant parameters we find $P_{a,a'}/P_a = 0.28 \pm 0.02$ and $\phi_{a,a'} = 130° \pm 10°$.

V. EXPERIMENTS ON KRYPTON

Krypton is the next noble-gas atom after argon and experimentally it has the important advantage that the $3d$ inner shell is energetically more easily accessible than the inner shells in argon. The binding energy of the $3d$ electrons is about 90 eV and the resulting Auger energies range from 25 to 55 eV. The important advantage is that at such relatively low photon and detection energies, the resolution of both the photon beam and the electron analyzer is much better than at higher energies.

In the experiment we have concentrated on the coherences between the photoionization of the $3d^{-1}(^2D_{3/2})$ (E_B=95.04 eV [22]) and the $3d^{-1}(^2D_{5/2})$ (E_B=93.79 eV [22]) inner-shell vacancy states. Similarly as before, these two states plus the corresponding photoelectrons can decay to the same final state, by tuning the photon energy hν such that in the following two processes:

$$h\nu + Kr \rightarrow Kr^+\ 3d^{-1}(^2D_{3/2}) + \underset{\ell=1,3}{e_{ph}^{(1)}} \rightarrow Kr^{2+}\ 4s^{-1}4p^{-1}(^1P_1) + \underset{\ell=1,3}{e_A^{(1)}} + \underset{\ell=1,3}{e_{ph}^{(1)}}$$

$$h\nu + Kr \rightarrow Kr^+\ 3d^{-1}(^2D_{5/2}) + \underset{\ell=1,3}{e_{ph}^{(2)}} \rightarrow Kr^{2+}\ 4s^{-1}4p^{-1}(^1P_1) + \underset{\ell=1,3}{e_A^{(2)}} + \underset{\ell=1,3}{e_{ph}^{(2)}},$$

the energy of the photoelectron $e_{ph}^{(1)}$ becomes equal to the energy of the Auger electron $e_A^{(2)}$, and, consequently, the energy of the photoelectron $e_{ph}^{(2)}$ becomes equal to the energy of the Auger electron $e_A^{(1)}$. Again, we have

to make sure that, in addition to their energies, also the orbital angular momenta of the photoelectrons and Auger electrons can be the same. From the processes above it can be seen that this condition is met for the two channels that we have chosen.

A. Experiment

The expected interference should be visible in the detection of the indistinguishable electrons $e_{ph}^{(1)}$ and $e_A^{(2)}$ on the one hand, and in the detection of the electrons $e_{ph}^{(2)}$ and $e_A^{(1)}$ on the other hand. We have chosen to study $e_{ph}^{(1)}$ ($3d_{3/2}^{-1}$ photoelectrons; E_B=95.04 eV) and $e_A^{(2)}$ ($M_5 - N_1N_{23}$ ($^1P_1$) Auger electrons at 37.67 eV [21]), rather than the other electron pair, because the electron yields of $e_{ph}^{(1)}$ and $e_A^{(2)}$ are of comparable size, which makes it easier to observe the effects of interference.

In preliminary measurements, similar to those discussed in the case of argon, the effects of interference appeared to be very small and, therefore, we have chosen for a different approach to look for the interference. Figure 4 shows the way in which we have performed the measurements. Again, the energies of photoelectrons and Auger electrons are shown as a function of the photon energy, with the Auger electrons represented by the horizontal line and the photoelectrons represented by the diagonal line. At the intersection of the two lines, the photoelectrons and Auger electrons become indistinguishable and the proposed interference is expected to occur. Several bold lines are drawn to indicate the way in which we have performed a number of so-called constant-energy-loss measurements. In each measurement the electron yield is recorded while varying the photon and the detection energy simultaneously, keeping the difference between the two energies, the energy loss ΔE, at a constant value. All the measurements contain a peak pertaining to the $M_5 - N_1N_{23}$ ($^1P_1$) Auger electrons. Moreover, if

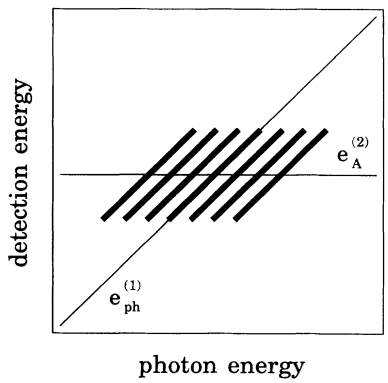

FIG. 4. The energies of photoelectrons ($e_{ph}^{(1)}$) and Auger electrons ($e_A^{(2)}$) as a function of the photon energy. At the intersection the proposed interference should be observable. The bold lines indicate the way in which we have performed a number of measurements in which the photon and the detection energy were varied simultaneously, keeping the difference between the two energies at a constant value, the so-called energy loss ΔE (see text).

ΔE is equal to the binding energy of the $3d_{3/2}$ inner-shell electrons (95.04 eV), the measurement will contain a continuous background of $3d_{3/2}^{-1}$ photoelectrons. The idea is that, going from measurements in which ΔE is slightly below 95.04 eV to measurements in which ΔE is slightly above 95.04 eV, the effects of interference will manifest themselves as systematic changes of the peak position of the Auger line. If interference plays no role, this peak position will occur at the same energy in all of the measurements schematically indicated in Fig. 4. However, looking again at, for instance, Fig. 1(c) or 1(d), it can be seen that if interference does play a role, the peak position of the Auger line may be shifted relative to the nominal position. Since the peak position of a line is one of the most accurate quantities that can be obtained from the measurements, it can be expected that this method is the most sensitive one to investigate the effects of interference.

The electron energy in the present experiment is typically 40 eV. By retarding these electrons to 10 eV, an energy resolution of 0.07 eV is achieved. The photon energy is typically 130 eV, with a bandwidth of about 0.04 eV.

B. Results and discussion

Figure 5 gives one of the many different constant energy-loss measurements, as indicated schematically in Fig. 4. The constant energy loss ΔE is equal to 94.74 eV in this case, 0.3 eV below the binding energy of the $3d_{3/2}$ inner-shell electrons. Since the background does, therefore, not contain photoelectrons, there should be no influence of interference. The measurement took about 15 minutes and it is clear that the peak position can be determined very accurately by making a linear least-squares fit of a Lorentzian profile to the data, of which the result is shown as a full curve in Fig. 5. The uncertainty in the determination of the peak position is about 0.002 eV and is mainly due to very small variations of the power supplies that provide the potentials on the CMA and the retarding spheres.

We have performed a total of three series of constant-

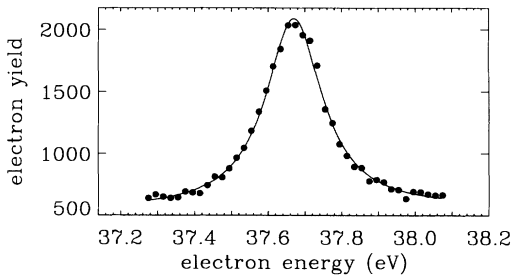

FIG. 5. The $M_5 - N_1N_{23}$ ($^1P_1$) Auger line of krypton as measured while varying the photon and the detection energy simultaneously, keeping the difference between the two energies equal to 94.74 eV. The full line indicates the result of a linear least-squares fit of a Lorentzian line shape on a linear background to the data.

energy-loss (CEL) measurements to study the interference effects. Each series contains a total number of 13 CEL spectra, in which the energy loss ΔE takes on the different values from 94.74 eV (0.3 eV below 95.04 eV) to 95.34 eV (0.3 eV above 95.04 eV) with steps of 0.05 eV. In the first series the different CEL spectra are measured for increasing values of ΔE, that is from left to right in Fig. 4. In the second series the different CEL spectra are measured for decreasing values of ΔE, that is from right to left, and in the third series the different CEL spectra are measured in random sequence. In this way we are sure that none of the observed changes in the peak positions could have been caused by possible drifts in the applied voltages.

Each of the three series showed a similar dependence of the peak position of the $M_5 - N_1N_{23}$ ($^1P_1$) Auger line as a function of the constant energy loss ΔE in the CEL measurement. The average of the three series is shown in Fig. 6. The uncertainties in the averaged peak positions are estimated to be about 0.0013 eV, i.e., $\sqrt{3}$ times smaller than the uncertainty of 0.002 eV as found for the individual CEL measurements. It can be seen that the peak position of the Auger line does depend on the value of ΔE. For values of ΔE slightly below 95.04 eV the dependence shows a positive energy shift relative to the nominal peak position of 37.67 eV of the Auger line, whereas for values of ΔE slightly above 95.04 eV the dependence shows a small negative energy shift. The effects of interference are indeed very small, as the energy difference between the largest positive and negative energy shifts is only about 0.01 eV, but the changes in the peak position are definitely outside the experimental uncertainties as indicated in Fig. 6.

The full curve in Fig. 6 is drawn according to the predicted dependence of the Auger peak position on the constant energy loss ΔE, as derived from our parametrized line shape (18). In a CEL measurement the reduced energy $\bar{\epsilon}_a$ is a constant, whereas the reduced energy $\bar{\epsilon}_{a'}$ is the parameter as a function of which the electron yield is measured. From Eq. (18) it can be seen that the dependence of the cross section on $\bar{\epsilon}_{a'}$ can also be written in the following way:

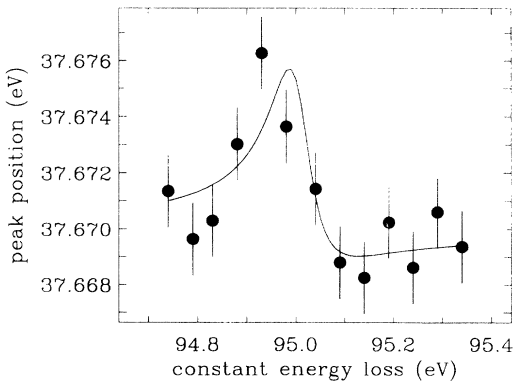

FIG. 6. The peak position of the $M_5 - N_1N_{23}$ ($^1P_1$) Auger line of krypton as a function of the constant energy loss ΔE, as obtained in a number of different constant energy-loss measurements. ΔE varies from 0.3 eV below to 0.3 eV above the binding energy of the $3d_{3/2}$ inner-shell electrons (95.04 eV).

$$\frac{d^2\sigma}{dEd\Omega} = C + \frac{A\bar{\epsilon}_{a'} + B}{\bar{\epsilon}_{a'}^2 + 1}, \tag{20}$$

in which the parameters A, B, and C are given by

$$A = Q^2 2P_{a,a'} \frac{\bar{\epsilon}_a \cos\phi_{a,a'} - \sin\phi_{a,a'}}{\bar{\epsilon}_a^2 + 1}, \tag{21}$$

$$B = Q^2 \left(2P_{a,a'} \frac{\cos\phi_{a,a'} - \bar{\epsilon}_a \sin\phi_{a,a'}}{\bar{\epsilon}_a^2 + 1} + 2P_{a'} \right), \tag{22}$$

$$C = Q^2 \frac{2P_a}{\bar{\epsilon}_a^2 + 1}. \tag{23}$$

It can be seen that the parameters A, B, and C do not depend on the reduced energy $\bar{\epsilon}_{a'}$, and, therefore, Eq. (20) is similar to the expression for a Fano profile in the Shore parametrization [26]. The reduced energy $\bar{\epsilon}_{\max}$ at which the profile reaches a maximum value can easily be derived from Eq. (20) to be

$$\bar{\epsilon}_{\max} = -\frac{B}{A} + \frac{1}{A}\sqrt{A^2 + B^2}. \tag{24}$$

Together with the expressions given above for A and B this gives us the reduced peak position $\bar{\epsilon}_{\max}$ of the Auger line, as a function of the reduced energy loss $\bar{\epsilon}_a$, with the parameters $P_{a'}$, $P_{a,a'}$, and $\phi_{a,a'}$.

To give some insight in the kind of dependence that is described by our Eq. (24), we will show that this equation is in fact a reasonable approximation to the expression for a Fano profile in the Shore parametrization [26]. If the amplitude $P_{a,a'}$ for the interference term is much smaller than the amplitude $P_{a'}$ pertaining to the Auger electrons, as seems to be the case in the present experiment on krypton, the value of B, as given in Eq. (22), will be much larger than the value of A, as given in Eq. (21). This implies that we can approximate the peak position $\bar{\epsilon}_{\max}$ as defined by (24), which yields

$$\bar{\epsilon}_{\max} \approx \frac{A}{2B} = \frac{P_{a,a'}(\bar{\epsilon}_a \cos\phi_{a,a'} - \sin\phi_{a,a'})}{2P_{a,a'}(\cos\phi_{a,a'} - \bar{\epsilon}_a \sin\phi_{a,a'}) + 2P_{a'}(\bar{\epsilon}_a^2 + 1)}.$$

If we neglect in the denominator of this expression the term proportional to $P_{a,a'}$, which is, as we have already seen, small as compared with $P_{a'}$, we finally arrive at

$$\bar{\epsilon}_{\max} = \frac{P_{a,a'}}{2P_{a'}} \frac{\bar{\epsilon}_a \cos\phi_{a,a'} - \sin\phi_{a,a'}}{\bar{\epsilon}_a^2 + 1}, \tag{25}$$

which can indeed be seen to be equal to a Shore profile [see Eq. (20)].

The full line in Fig. 6 is drawn according to the nonapproximated Eq. (24) and by using the values $P_{a'}/P_{a,a'} = 75$, $\phi_{a,a'} = 135°$ and $\Gamma_a = 0.11$ eV. It can be seen that there is a good agreement between the experimental results and the predicted dependence on the energy loss. Because of the limited number of data points we have not tried to fit with a computer the dependence (24) to

the data. The given fit has been determined by outwardly looking for the best curve through the data, the corresponding value of χ^2 being equal to 0.93. In the same way we are also able to establish the uncertainties in the given values of the parameters, and we arrive at $P_{a'}/P_{a,a'} = 75 \pm 13$, $\phi_{a,a'} = 135° \pm 18°$, and $\Gamma_a = 0.11 \pm 0.04$ eV. The latter value is within the experimental uncertainty equal to the natural linewidth of 0.10±0.01 eV as given by Svensson *et al.* [27] and the value of 0.098±0.012 eV as given by King *et al.* [22]. Of course, the measured width is influenced by the transmission profile of the electron analyzer and the energy profile of the photon beam. However, since the width of both apparatus profiles is narrower than the measured width, we assume that their influence is only small, as in the case of argon.

VI. CONCLUSION AND FUTURE

We have observed the coherence between the photoionization of different inner-shell vacancy states of argon and krypton. This coherence could be observed by measuring interferences between photoelectrons and Auger electrons. The resulting interference effects can qualitatively be well described using a simplified version of the theory as given by van den Brink *et al.* [9].

More work is needed in the future to understand also quantitatively the presently observed interference effects. Theoretically, it seems feasible to perform *ab initio* calculations to explain quantitatively the presently observed interference phenomena. The present experiments provide an important test on a very fundamental level for such calculations.

The present method of noncoincident detection of the electrons can be used to gain further information on the interference. Consider again the scheme as given in Eq. (2). The present experiments have paid attention to the interference effects that occur in the detection of one electron pair, for instance $e_{\rm ph}^{(1)}$ and $e_A^{(2)}$, if the photon energy is chosen such that these electrons have the same energy. The interference in the detection of the alternative electron pair, $e_{\rm ph}^{(2)}$ and $e_A^{(1)}$, should give complementary information. Moreover, it should also be possible, at another photon energy, to observe interference between $e_{\rm ph}^{(1)}$ and $e_A^{(1)}$, and, at yet another photon energy, to observe interference between $e_{\rm ph}^{(2)}$ and $e_A^{(2)}$, that is between the photoelectrons and Auger electrons resulting from the photoionization process of the same inner-shell vacancy state. A first attempt to observe interference effects of this kind has been described by Schmidt [28]. These experiments should also give complementary information and hence it should be possible to determine from the experiment the phases pertaining to the coherence in the photoionization process separately from the phases pertaining to the Auger decay.

A much more advanced experiment would involve a coincident detection of the electrons $e_{\rm ph}^{(1)}$ and $e_A^{(2)}$ on the one hand, and $e_{\rm ph}^{(2)}$ and $e_A^{(1)}$ on the other hand. In the near future such coincidence experiments should be feasible using the next-generation synchrotron-radiation sources, such as the Advanced Light Source in Berkeley and the synchrotron in Trieste which have recently become available.

ACKNOWLEDGMENTS

This work is part of the research program of the Stichting voor Fundamenteel Onderzoek der Materie (FOM), which is financially supported by the Nederlandse Organisatie voor Wetenschappelijk Onderzoek (NWO). The authors would like to thank Dr. J.B. West and Dr. M.D. Roper of the Daresbury Laboratory for useful help in planning and preparing the experiments.

[1] N. Andersen, J.W. Gallagher, and I.V. Hertel, Phys. Rep. **165**, 1 (1988).
[2] H. Andrä, Phys. Scr. **9**, 257 (1974).
[3] F.H. Read, J. Phys. B **10**, L207 (1977).
[4] H.G.M. Heideman, *Coherence and Correlation in Atomic Collisions* (Plenum, New York, 1980), p. 493.
[5] A. Niehaus, *Atomic Inner-Shell Physics* (Plenum, New York, 1985), p. 377.
[6] N.L.S. Martin and D.B. Thompson, Phys. Rev. A **43**, 2281 (1991).
[7] N.L.S. Martin, D.B. Thompson, R.P. Bauman, and M. Wilson, J. Phys. IV **3**, C6-69 (1993).
[8] J.P. van den Brink, J. van Eck, and H.G.M. Heideman, Phys. Rev. Lett. **61**, 2106 (1988).
[9] J.P. van den Brink, G. Nienhuis, J. van Eck, and H.G.M. Heideman, J. Phys. B **22**, 3501 (1989).
[10] J.P. van den Brink, P.N. den Outer, J. van Eck, and H.G.M. Heideman, J. Phys. B **23**, 2349S (1990).
[11] J.A. de Gouw, J. van Eck, A.C. Peters, J. van der Weg, and H.G.M. Heideman, Phys. Rev. Lett. **71**, 2875 (1993).
[12] L. Végh and J.H. Macek, Phys. Rev. A (to be published).
[13] L. Végh L, Phys. Rev. A (to be published).
[14] U. Fano, Phys. Rev. **124**, 1866 (1961).
[15] U. Fano and J.W. Cooper, Phys. Rev. **137**, A1364 (1965).
[16] T. Åberg and G. Howat, *Encyclopedia of Physics* (Springer-Verlag, Heidelberg, 1982), Vol. 31, p. 469.
[17] S. Svensson, N. Mårtensson, and U. Gelius, Phys. Rev. Lett. **58**, 2639 (1987).
[18] L. Journel, B. Rouvellou, D. Cubaynes, J.M. Bizau, F.J. Wuilleumier, M. Richter, P. Sladeczek, K.-H. Selbmann, P. Zimmerman, and H. Bergeron, J. Phys. IV **3**, C6-217 (1993).
[19] M. Borst and V. Schmidt, Phys. Rev. A **33**, 4456 (1986).
[20] J.A. de Gouw, A.C. Peters, J. van Eck, J. van der Weg, and H.G.M. Heideman, J. Electron Spectrosc. **63**, 379 (1993).

[21] K. Siegbahn, C. Nordling, G. Johansson, J. Hedman, P.F. Hedén, K. Hamrin, U. Gelius, T. Bergmark, L.O. Werme, R. Manne, and Y. Baer, *ESCA Applied to Free Molecules* (North-Holland, Amsterdam, 1969), p. 23.
[22] G.C. King, M. Tronc, F.H. Read, and R.C. Bradford, J. Phys. B **10**, 2479 (1977).
[23] G. Johansson, J. Hedman, A. Berndtsson, M. Klasson, and R. Nilsson, J. Electron Spectrosc. **2**, 295 (1973).
[24] P. Glans, R.E. LaVilla, M. Ohno, S. Svensson, G. Bray, N. Wassdahl, and J. Nordgren, Phys. Rev. A **47**, 1539 (1993).
[25] Kh.R. Karim, M.H. Chen, and B. Crasemann, Phys. Rev. A **29**, 2605 (1984).
[26] B.W. Shore, Rev. Mod. Phys. **39**, 439 (1967).
[27] S. Svensson, N. Mårtensson, E. Basilier, P.A. Malmquist, U. Gelius, and K. Siegbahn, Phys. Scr. **14**, 141 (1976).
[28] V. Schmidt, Nucl. Instrum. Methods Phys. Res. Sect. B **87**, 241 (1994).